

JBC Turbulence

Aim

The Japan Bulk Carrier (JBC) Turbulence Test Case will focus on the physical understanding of the mean and unsteady flow, 3D vortex separation onset and progression, and turbulence structure for ship flows. The specific interest is on anisotropic RANS and Scale Resolving Simulation (SRS) methods and their simulation of the flow in the propeller and rudder regions. The test cases will use the conditions of the T2015 (<https://t2015.nmri.go.jp/>) JBC 1.1a (Case 1) and 1.3a (Case 2) with expanded analysis, including steady and unsteady primary and secondary vortex core analysis of the turbulence realizability and anisotropy and Taylor macro and micro scales and Kolmogorov spectrums. All the available experimental data will also be assessed and used for the validation along with model spectrums based on the macro scales for both the experiments and simulations. Case 2 will be for fixed sinkage and trim at the experimental values. Case 0 is preliminary to Cases 1 and 2 and covers issues related to the grid distributions, iterative and statistical convergence, and SRS deficiencies and errors. Anisotropic RANS submissions must include the free surface for Cases 0 and 1. If possible, SRS submissions should include both RANS (isotropic or anisotropic are acceptable) and SRS on the same grids for Cases 0, 1, and 2 and for codes that do not have free surface capability double body simulations at zero sinkage and trim will also be accepted for only Cases 0 and 2.



Figure 1: JBC Resistance Test in NMRI Towing Tank.

Approach

The approach builds on the T2015 JBC (Figure 1 and Table 1) test cases 1.1a (Case 1) and 1.3a (Case 2), as shown in Table 2 and Table 3, but with focus on the assessment of anisotropic RANS and SRS. The wave pattern analysis is included in Case 1 and 2.

The conditions for Case 1 are for free sinkage and trim $FR_{z\theta}$, whereas for Case 2 they are for fixed sinkage and trim $FX_{z\theta}$ at the experimental values¹. Double body submissions at the same Reynolds number with post facto adjustment for sinkage and trim are also acceptable. However, this should only be the case for codes that do not have free surface capability, since the condition with free surface is very much preferred for ship hydrodynamics. An updated IGES file is provided that includes the dummy hub and hub cap. Figure 2 shows the coordinate system.

¹ This differs from T2015 which also used $FR_{z\theta}$ for test case 1.3a.

Table 1: Principal particulars of full scale, NMRI, OU, and CSSRC models

		Full scale	NMRI	OU	CSSRC
Length between perpendiculars	$L_{pp}(m)$	280.0	7.000	3.200	3.513
Length of waterline	$L_{WL}(m)$	285.0	7.125	3.257	3.576
Maximum beam of waterline	$B_{WL}(m)$	45.0	1.1250	0.5143	0.565
Displacement volume	$\nabla(m^3)$	178369.9	2.787	0.2663	0.3523
Depth	$D(m)$	25.0	0.6250	0.2857	-
Draft	$T(m)$	16.5	0.4125	0.1886	0.208
Wetted surface area	$S(m^2)$	19556.1	12.223	2.554	3.0784
Block coefficient	C_B	0.8580	0.8580	0.8580	0.8580
Midship section coefficient	C_M	0.9981	0.9981	0.9981	0.9981
LCB (% L_{pp}), forward of midship		2.55	2.55	2.55	-
Vertical center of gravity (from keel)	KB (m)	13.29	0.3323	0.1519	-
Turbulence stimulation		-	Two rows of studs at 75.0mm ahead of FP and 350.0mm aft of FP	Two rows of studs at 34.3mm ahead of FP and 160.0mm aft of FP	Three trip wires at 50.0mm ahead of FP, 175.6mm aft of FP and 309.1mm aft of FP

Table 2: Test cases

Case	Hull	Condition	Attitude	Validation variables	Data provider
Case 0	JBC	Towed in calm water	$FX_{z\theta}^2$	Grid resolution analysis	
Case 1	JBC	Towed in calm water	$FR_{z\theta}$	Focus: Resistance, sinkage and trim, and wave pattern	NMRI, OU, CSSRC
Case 2	JBC	Towed in calm water	$FX_{z\theta}$	Focus: Mean and unsteady flow and turbulence structure	NMRI, OU, CSSRC

² For double body submissions FX at zero sinkage and trim is acceptable.

Table 3: Results of resistance test at design speed

		NMRI	OU
Model speed	$V_m (m/s)$	1.179	0.795
Froude number	$F_n = \frac{V_m}{\sqrt{gL_{pp}}}$	0.142	0.142
Reynolds number	$R_n = \frac{V_m L_{pp}}{\nu}$	$7.46 \times 10^{6,3}$	2.17×10^6
Total resistance coefficient	$C_T = \frac{R_T}{0.5\rho V_m^2 S}$	4.29×10^{-3}	5.27×10^{-3}
1 + Form factor	$1 + k$	1.314	1.26
Wave making resistance coeff.	$C_W = \frac{R_W}{0.5\rho V_m^2 S}$	1.5×10^{-4}	2.447×10^{-4}
ITTC 1957 correlation line	C_{F0}	3.163×10^{-3}	3.988×10^{-3}
Sinkage (+:upward)	sinkage/ L_{pp} (%)	-8.57×10^{-2}	-7.65×10^{-2}
Trim (+:bow-up)	trim (%)	-1.80×10^{-1}	-1.75×10^{-1}
Gravity	$g (m^2/s)$	9.80	9.80
Density of water	$\rho (kg/m^3)$	998.2	999.6
Kinematic viscosity of water	$\nu (m^2/s)$	1.107×10^{-6}	1.172×10^{-6}

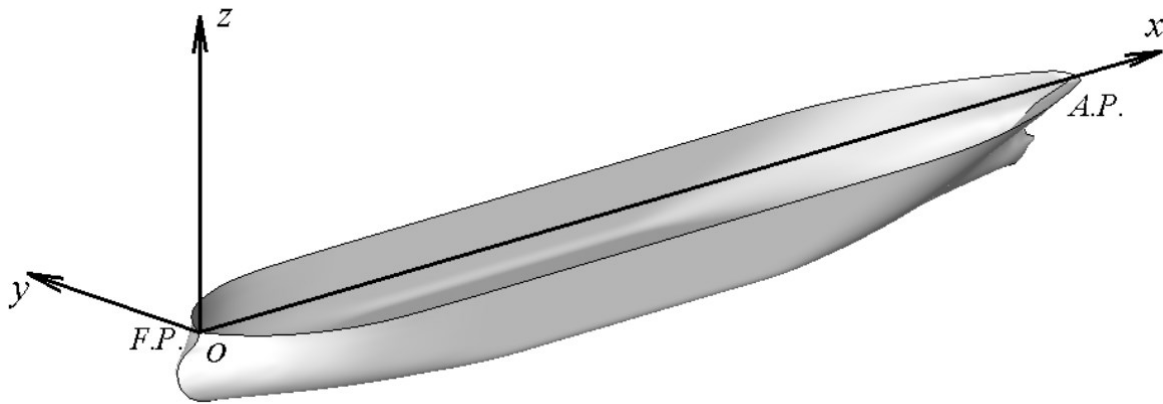


Figure 2: Coordinates system.

³ Note Resistance test NMRI done at $Re = 7.569 \times 10^6$ and PIV at $Re = 7.46 \times 10^6$. Herein PIV Re is used for both Cases 1 and 2.

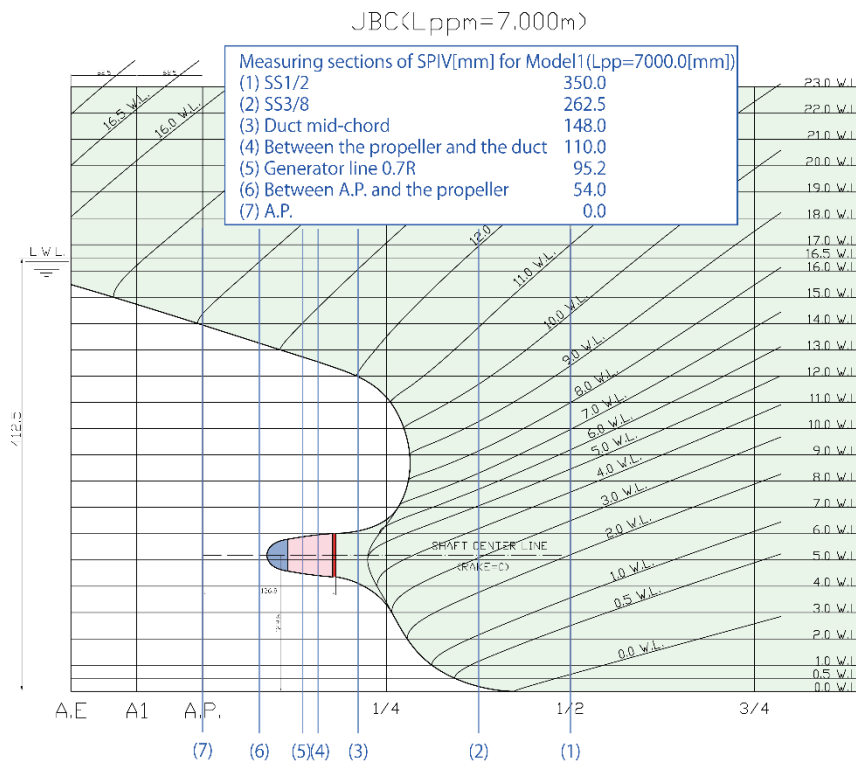


Figure 3: JBC stations for the assessment of the experimental data and anisotropic RANS and SRS.

The attention is on stations S2, S4, and S7, as shown in Figure 3, and the larger ABV1 and smaller ABV2 vortices, as shown in Figure 4, for realizability and anisotropy and SRS detailed analysis especially for S4.

All the available experimental data will be collected (e.g., Figure 4) and evaluated and used for the CFD assessment. There are two major drawbacks regarding the experiments:

- (1) Large scatter of the available data, as per T2015 proceedings and Zheng et al. (2024)
- (2) Minimal available Reynolds Stress (RS) and time series data.

Therefore, the assessments will also be based on the physics and on the comparisons among submissions for realizability and anisotropy; and for macro and micro scale analysis, which will also use model spectrums based on the macro scales for both the experiments and SRS for benchmarking. The analysis methods will follow those used by Stern et al. (2024).

Case 0 is preliminary to Cases 1 and 2 and covers issues related to the grid distributions, iterative and statistical convergence, and SRS deficiencies and errors with particular attention on modelled stress depletion (MSD) and grid induced separation (GIS) to aid in the development of best practices for potentially resolving these issues.

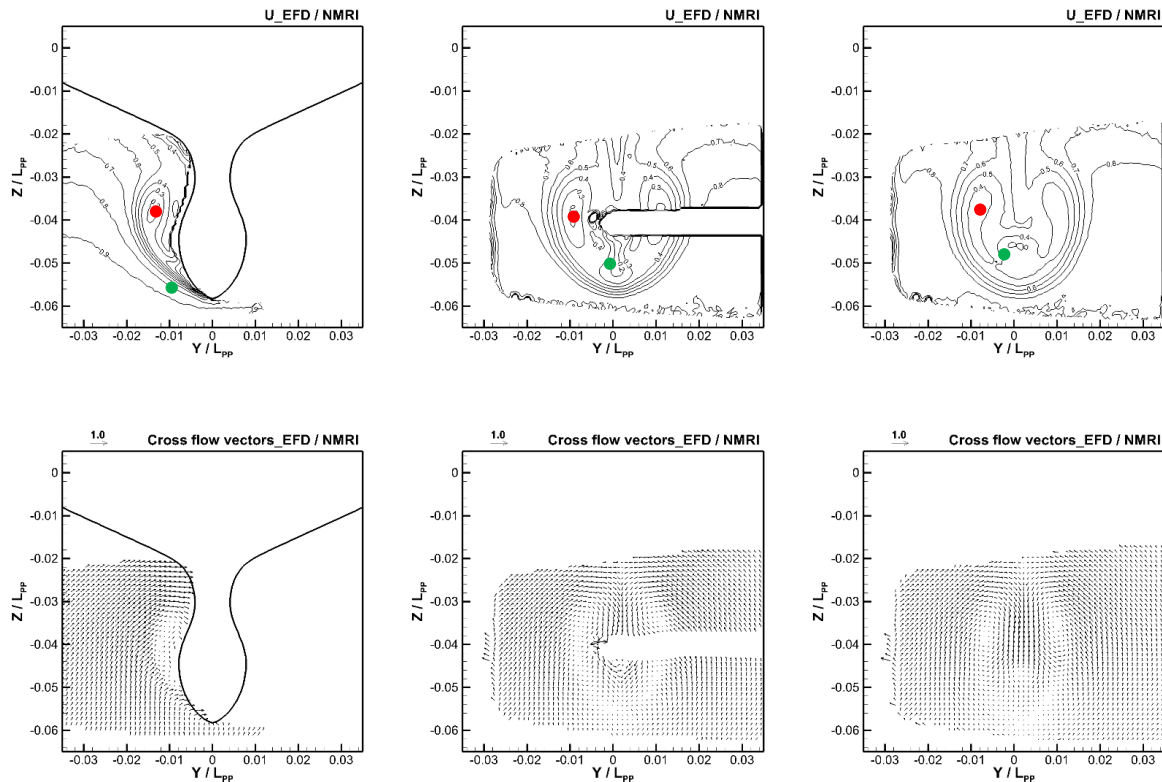


Figure 4: U contours and VW vectors at S2 (left), S4 (middle), and S7 (right): NMRI data: upper larger vortex is ABV1 (●), and lower smaller vortex is ABV2 (●).

Submission Variables and Instructions

An overview of the submission variables and instructions is provided below for Cases 0, 1, and 2. The detailed format for the submissions is still under development and will be provided soon; however, the present description should be sufficient for the participants to initiate their setups and simulations. Any questions and/or concerns should be emailed to the organizers who will quickly provide answers and any necessary updates: <mailto:w2025@marin.nl?subject=JBC>.

Case 0: Grid Distributions, Iterative and Statistical Convergence, and SRS Deficiencies and Errors

Refer to Appendix A for details of the plots requested.

0.1. Plots for grid scale distribution

- 0.1.1 Grid density distribution along the waterline, and in transverse and vertical directions.
- 0.1.2 Grid distribution and grid-scale and macro/micro-scale ratio contours at section S2, S4 and S7.
- 0.1.3 Zoom in view of the grid distribution w/ flooded contour of the ratio of turbulence macro-scale (L) and grid-scale D , and contour line of $y^+ = 30, 100, 300$ and 1000 at S2.

0.2. Iterative convergence of the solution

0.3. Integral Variable Solution convergence

0.4. Statistical convergence of SRS results

- 0.4.1 Time history of the axial velocity and resolved TKE along with the running mean in ABVI and ABV2 cores at S4.
- 0.4.2 Statistical convergence of mean velocity resolved TKE in ABVI and ABV2 core at S4.

0.5. SRS deficiency/error analysis

- 0.5.1 Longitudinal distribution of the viscous and pressure girthwise integrated resistance.
- 0.5.2 Iso-surfaces of the RANS and grid-scale ratio or DES shielding function in the wake using isovalue of 0.99.
- 0.5.3 2D slices at section S2, S4 and S7 showing contour of scale ratio and shielding function
- 0.5.4 2D slices at sections S2, S4 and S7 showing resolved and modeled TKE levels
- 0.5.5 Line cuts at one location at S1 ($x/L = 0.95$) three locations at S2 ($x/L = 0.9625$) comparing HRLES and RANS mean velocity and TKE in the boundary layer, and ratio of RANS TKE and HRLES modeled TKE

Case 1: Resistance, Sinkage and Trim and Wave Pattern

1.1 Resistance (total, pressure and friction: C_T , C_p , C_f) Sinkage and trim

$$\text{Where } C_T = \frac{R_T}{0.5\rho V_m^2 S}, C_p = \frac{R_p}{0.5\rho V_m^2 S}, C_f = \frac{R_f}{0.5\rho V_m^2 S}$$

with R_T , R_p and R_f being total resistance, pressure resistance and frictional resistance.

Sinkage (%) and trim (% L_{pp}) are

$$\text{Sinkage} = -\frac{(d_f + d_a)}{2L_{pp}} \times 100, \text{Trim} = \frac{(d_a - d_f)}{L_{pp}} \times 100$$

with d_f and d_a are dipping (+: downward) at FP and AP, respectively.

1.2 Wave Contours

1.3 Wave Profile

1.4 Longitudinal Wave Cuts

1.4.1 $y/L = -0.1043$

1.4.2 $y/L = -0.1900$

Case 2: Resistance, Mean and Unsteady Flow and Turbulence Structure

2.0 Resistance, z force, and pitch moment⁴

- 2.0.1 Resistance (total, hydrodynamic pressure, and friction: C_T , C_p , C_f), z force (total pressure and friction forces), and pitch moment⁵; for both RANS and SRS submissions on same grid unless pure LES used. See 1.1 for the definitions of resistance coefficients.

⁴ Double body submissions need only submit results for 2.0.1, whereas for submissions with free surface capability wave contour, profile and longitudinal cuts required to ensure same quality as Case 1.

⁵ Z force and pitch moment integration should include the deck.

2.0.2 Wave Contours

2.0.3 Wave Profile

2.0.4 Longitudinal Wave Cuts

2.0.4.1 $y/L = -0.1043$

2.0.4.2 $y/L = -0.1900$

2.1 Anisotropic RANS flow: mean flow and vortex structures; Reynolds stresses and their realizability and anisotropy

2.1.1 Mean Surface Flow

2.1.1.1 Pressure (c_p) with surface streamlines (Ψ_0).

2.1.1.2 Shear stress $\left(\frac{\tau_w}{0.5\rho V_m^2}\right)$.

2.1.2 Mean 3D Vortex Structure and ABV1 and ABV2 Core Analysis

2.1.2.1 3D views of the mean vortex structure with focus ABV1 and ABV2.

2.1.2.2 Show their cores connecting to the surface streamlines separation points (onset) and progression to their exit from S7. Singular point analysis at vortex onset.

2.1.2.3 Document the ABV1 and ABV2 core locations at S2, S4, and S7.

2.1.3 Planar mean contours

2.1.3.1 \mathbf{V} , C_p , TKE, RS contours at $x/L = 0.5$

2.1.3.2 \mathbf{V} , C_p , TKE, RS contours at S2

2.1.3.3 \mathbf{V} , C_p , TKE, RS contours at S4

2.1.3.4 \mathbf{V} , C_p , TKE, RS contours at S7

where

$$\mathbf{V} = \left(\frac{u}{V_m}, \frac{v}{V_m}, \frac{w}{V_m} \right)$$

$$C_p = \frac{p}{0.5\rho V_m^2}, TKE = \frac{k}{V_m^2}, RS = \left(\frac{u'u'}{V_m^2}, \frac{v'v'}{V_m^2}, \frac{w'w'}{V_m^2}, \frac{u'v'}{V_m^2}, \frac{u'w'}{V_m^2}, \frac{v'w'}{V_m^2} \right)$$

2.1.4 Mean ABV1 and ABV2 Vortex Analysis

2.1.4.1 w_x contours with Q isolines for ABV1 and ABV2 at S2, S4⁶, and S7, including YY and ZZ cuts through the vortex core and outline for viewing window pertaining to 3D perspective views.

2.1.4.2 Determine ABV1 and ABV2 diameter D ($R = D/2$) based on $Q = 0$ contour⁷.

2.1.4.3 Q/Q_{max} and $w/w_{x,max}$ vs. r/R and comparisons with Gaussian and Bell distributions for YY and ZZ cuts.

⁶ S4 will be mandatory, whereas S2 and S7 are under consideration and need additional thought and discussion. Main concern is that the analysis will be too much, and the assessment of the submissions will be overwhelming.

⁷ Note that AVT-253 defined the vortex core width as the average of the height and width of the iso-surface of $Q'_{max/2}$, with Q'_{max} the maximum Q value in the vortex core.

- 2.1.4.4 Q/Q_{\max} 3D contours with mesh overlay.
- 2.1.4.5 Evaluate the ABV1 and ABV2 circulation and swirl numbers using line integral and normal vorticity ω_n flux⁸.
- 2.1.4.6 Reynolds stresses and anisotropy analysis for ABV1 and ABV2 for S2, S4, and S7, including Lumley triangle and Reynolds stress ellipsoid.
- 2.1.4.7 Macro-scale vortex core parameters for ABV1 and ABV2 for S2, S4, and S7, as per Table 4.

Table 4: Macro Scale Variables (see Stern et al. 2024 for definitions).

Parameter
$\langle U \rangle$ [m/s]
$\langle u^2 \rangle$ [m ² /s ²]
$k = \frac{1}{2}(\langle u^2 \rangle + \langle v^2 \rangle + \langle w^2 \rangle)$ [m ² /s ²]
$u' = (2/3k)^{1/2}$ [m/s]
$L = D$ [m] = diameter vortex for ABV1 and ABV2
$\varepsilon = k^{3/2}/L$ [m ² /s ³]
$Re_L = k^{1/2}L/\nu$
l_f [m] = $\sqrt{20}LRe_L^{-\frac{1}{2}}$,
$R_i = \frac{k^{1/2}\lambda_f}{\sqrt{2}\nu}$
$h = \left(\frac{v^3}{\varepsilon}\right)^{\frac{1}{4}}$ [mm]

2.2 Scale resolved flow: for ABV1 and ABV2 at S2, S4, and S7

- 2.2.1 $u(x, t)$ time histories at vortex cores for ABV1 and ABV2 at S2, S4, and S7, including FFT and analysis organized oscillation analysis⁹.
- 2.2.2 $u(x, t)$ along vortex cores upstream and downstream of vortex cores for ABV1 and ABV2 at S2, S4, and S7, including contour maps and analysis Taylor Frozen Turbulence Hypothesis¹⁰.
- 2.2.3 Temporal micro and macro (via autocorrelation analysis) scales, Taylor Frozen Turbulence Hypothesis, energy and Kolmogorov spectrums. Benchmark model spectrum based on micro scales k and $\varepsilon = \frac{30\nu u'^2}{\lambda_f^2}$, as per Table 5.
- 2.2.4 Symmetric and antisymmetric spatial micro and macro (via autocorrelation analysis) scales, energy and Kolmogorov spectrums. Benchmark model spectrum based on micro scales k and $\varepsilon = \frac{30\nu u'^2}{\lambda_f^2}$, as per Table 5.
- 2.2.5 Benchmark model spectrum based on macro scales $k = TKE$ and $\varepsilon = k^{3/2}/L$, as per Table 4.

⁸ Detailed instructions in preparation will follow Stern et al. (2024).

⁹ Δt and period T (duration) for submissions to be specified.

¹⁰ Δr and upstream and downstream lengths to be specified.

- 2.2.6 3D views unsteady/instantaneous vortex structures and vortex cores; FFT unsteady vortex cores: details to be provided.
- 2.2.7 Vortex-vortex interaction analysis ABV1 and ABV2: details to be provided.

Table 5: Micro Scale Variables with benchmark model spectrums for both macro and micro scale analysis (see Stern et al. 2024 for definitions).

Parameter
$\lambda_f = \sqrt{20}LR_L e_L^{-0.5}$ [mm]
$L_f = L_{11}$ [mm]
$R_\lambda = \frac{k^{0.5}\lambda_f}{\sqrt{2\nu}}$
$\varepsilon = \frac{30\nu u'^2}{\lambda_f^2}$ [m ² /s ³]
$\eta = \left(\frac{\nu^3}{\varepsilon}\right)^{\frac{1}{4}}$ [mm]

The 3D model spectrum is defined as:

$$E(\kappa) = C\varepsilon^{\frac{2}{3}}\kappa^{-\frac{5}{3}}f_L(\kappa L)f_\eta(\kappa\eta),$$

$$f_L(\kappa L) = \left(\frac{\kappa L}{[(\kappa L)^2 + c_L]^{\frac{1}{2}}}\right)^{\frac{5}{3}+p_0},$$

$$f_\eta(\kappa\eta) = \exp\left\{-\beta\left\{[(\kappa\eta)^4 + c_\eta^4]^{\frac{1}{4}} - c_\eta\right\}\right\},$$

$$L_{11} = \frac{3\pi}{4k} \int_0^\infty \frac{E(\kappa)}{\kappa} d\kappa,$$

References

Pope, S. B., Turbulent Flows, Cambridge Univ. Press, 2000.

Sanada, Y., Starman, Z., Bhushan, S., and Stern, F. "Four-Dimensional Particle Tracking Velocimetry Measurements of Unsteady Three-Dimensional Vortex Onset and Progression for 5415 Straight Ahead, Static Drift, and Pure Sway". Phys. Fluids 35, 105125, 2023. doi: 10.1063/5.0165658.

Stern, F., Sanada, Y., Starman, Z., Bhushan, S., and Milano, C., "4DPTV Measurements and DES of the Turbulence Structure and Vortex-Vortex Interaction for 5415 Sonar Dome Vortices," 35th Symposium on Naval Hydrodynamics, Nantes, France, 7 July - 12 July 2024. [🔗](#)

Yoon, H., Longo, J., Toda, Y., and Stern, F., "Benchmark CFD Validation Data for Surface Combatant 5415 in PMM Maneuvers—Part 2: Phase-Averaged SPIV Flow Field Measurements," Ocean Eng. 109, 735, 2015.

Zheng, W. et al., "SPIV Measurement of Flowfield after Japan Bulk Carrier at Straight Ahead Condition in Wind Tunnel," Journal of Shipbuilding of China, Vol. 65, 2024 (in Chinese).

Appendix A. Details of Case 0: Grid Distributions, Iterative and Statistical Convergence, and SRS Deficiencies and Errors

0.1 Plots for grid scale distribution

Grid distribution can help evaluate the grid topology used to resolve the boundary layer, how the grid transitions in the wake region. The distribution of grid-scale in the boundary layer and in the wake also helps evaluate how well the micro and macro turbulent scales are resolved. RANS simulations should have grid scales that are fine enough to resolve the macro-scale, and SRS should have grid scales that lie within the inertial subrange.

The length scales associated with turbulence are summarized in Figure A.1 below. They can be portioned as large-scale energy containing scale, where the turbulence production occurs. Inertial subrange, where the turbulent energy cascades to smaller length scales without any dissipation. Dissipation subrange where the energy decays because of molecular viscosity.

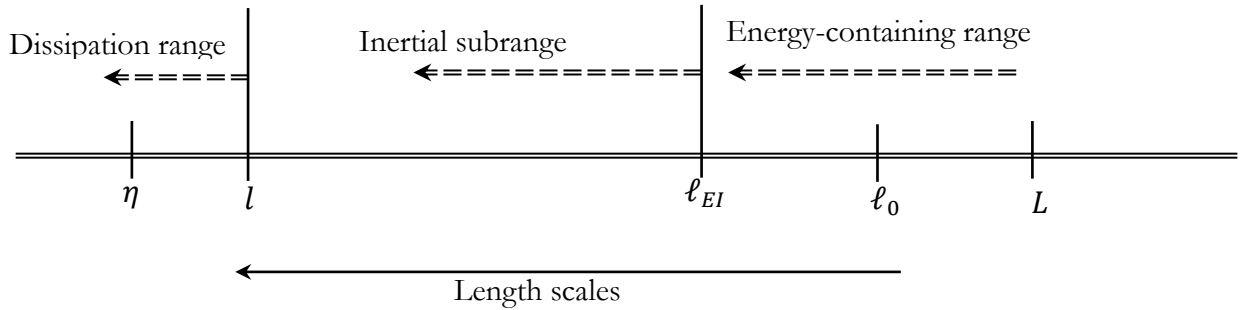


Figure A.1: Schematic view of eddy sizes ℓ showing the various length-scale of turbulence from smaller to larger (left to right). Taken from Pope (2000), Fig. 6.1. Arrows show the energy transfer pathway.

The length scales associated with energy containing range from turbulence macro-scale $L \approx \frac{k^{3/2}}{\varepsilon}$, which is $\approx 6l_0$, where $l_0 = 0.1643k^{3/2}/\varepsilon$ is turbulent mixing length scale captured in (U)RANS (Pope, 2000). Note that for k- ω turbulence model $\varepsilon = C_\mu k\omega$, $C_\mu = 0.09$. The lower end of the energy-containing range is the start of the inertial subrange, which is estimated as $\ell_{EI} \approx 1/6l_0$. The inertial subrange extends up to Taylor's microscale. Note that Taylor's microscales are defined as scales below which the molecular dissipation becomes important. The dissipation subrange extends up to the Kolmogorov length-scale $\eta = LRe_L^{-3/4}$. Note that Pope (2000) also introduced $l_{DI} \sim 60\eta$ as the start of the dissipation range. We can estimate that $l_{DI} \sim l$ for $Re_L \sim 10^5$.

In (U)RANS, the grid scale ($D = \sqrt[3]{V}$, where V is grid volume) should lie in between $\ell_{EI} < \Delta < L$. The best resolution for accurate prediction of energy containing range is when $\Delta \rightarrow \ell_{EI}$. For proper resolution of the largest energy containing eddies, $\frac{L}{\Delta} > 10$, i.e., more than 10 grid cells to resolve the vortical structures.

In SRS, the grid scale should lie in the inertial subrange $l < \Delta < \ell_{EI}$. The best resolution for accurate prediction of energy containing range is when $\Delta \rightarrow \ell_{EI}$. The finest SRS resolution is when $\Delta \rightarrow l$.

Each submission should provide the following plots:

- (a) Grid density distribution along the waterline, and in transverse and vertical directions at mid-ship following T2015, as shown in Figure A.2. The figure should show:

- (i) Number of cells per fundamental wavelength in longitudinal direction at $y/L_{PP} = -0.1043$

$$ppwl = \frac{2\pi F_n^2}{\Delta x/L_{PP}} \text{ vs. } x/L_{PP}, \text{ where } -0.25 \leq x/L_{PP} \leq 1.25 \text{ using solid line.}$$

- (ii) Number of cells per fundamental wavelength in transverse direction at midship, along y axis and at the still water plane level:

$$ppwl = \frac{2\pi F_n^2}{\Delta y / L_{PP}} \text{ vs. } y / L_{PP} \text{ where } 0.25 \leq y / L_{PP} \leq 1.25 \text{ using dashed line.}$$

- (iii) Nondimensionalized cell size in vertical direction at midship and $y / L_{PP} = -0.1043$ along z axis:

$$\Delta y / L_{PP} \text{ vs } z / L_{PP} \text{ where } -0.01 \leq z / L_{PP} \leq 0.01 \text{ using dashed-dotted line.}$$

Sample plot shown in Figure A.2.

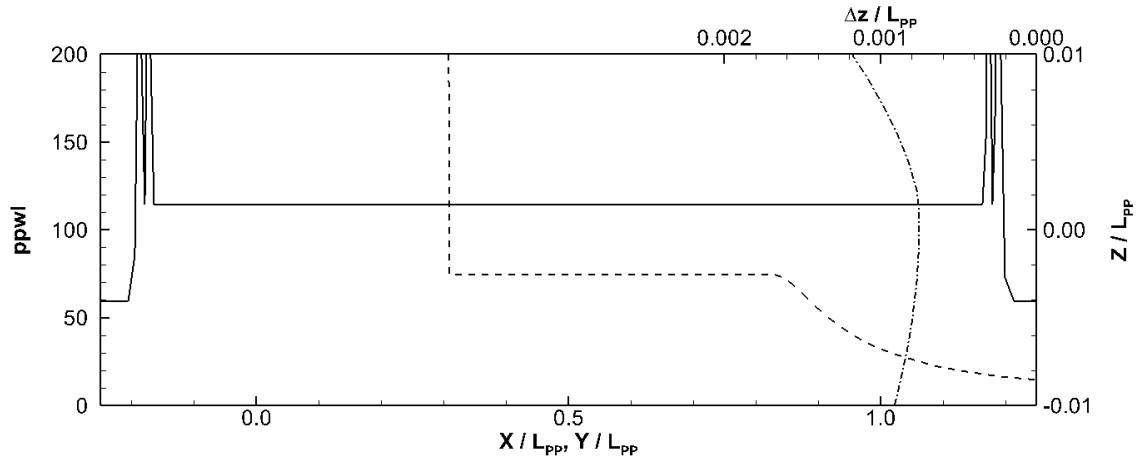


Figure A.2: Grid density distribution following T2015.

- (b) Grid distribution and grid-scale and macro/micro-scale ratio contours at section S2, S4 and S7. The definitions of the macro- and micro-scales are provided by Stern et al. (2024). Plots should be shown for:

- (i) Grid lines and ratio of turbulent macro-scale (L) and grid-scale as shown in Figure A.3.
- (ii) Grid lines and ratio of largest length-scale of the inertial subrange (l_{EI}) and grid-scale.
- (iii) Grid lines and ratio of grid-scale and estimated Taylor's micro-scale (λ).
- (iv) Grid lines and ratio of grid-scale and estimated dissipation length scale (η).

URANS submissions should show only (i) and (ii) to demonstrate how well the energy-containing scales were resolved. SRS submissions should show (ii), (iii) and (iv) to demonstrate how well the inertial subrange was resolved.

Sample figures are shown in Figure A.3.

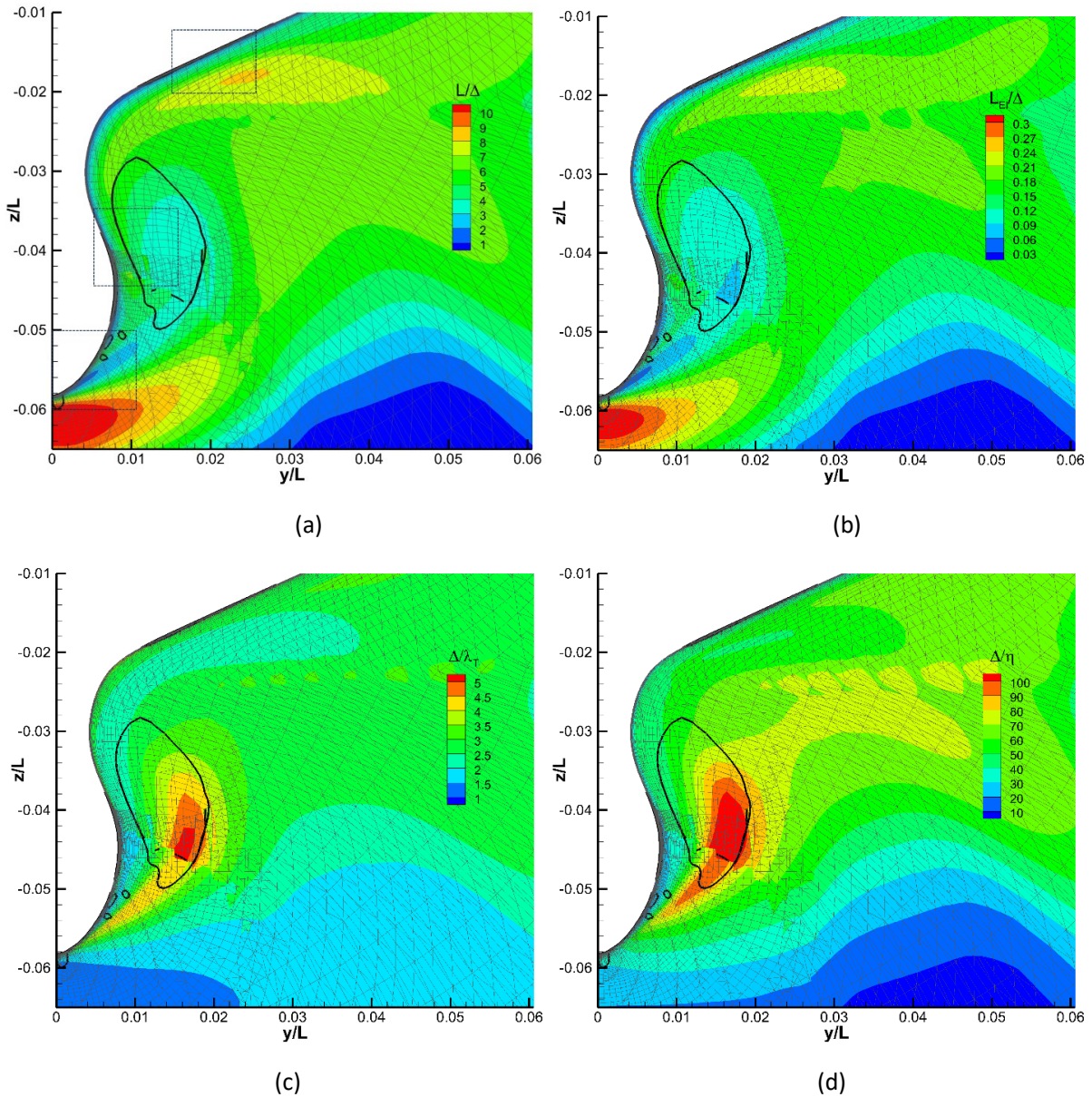


Figure A.3: (a) Grid distribution and contours of the ratio of turbulent macro-scale (L) and grid-scale, $D = \sqrt[3]{V}$, where V is grid volume, along with contour line (thick black line) of $Q = 100$. The regions shown with broken lines are for the zoomed in plots. (b) Grid distribution and contours of ratio of largest length-scale of the inertial subrange (l_{EI}) and grid-scale D , along with $Q = 100$ contour line. (c) Grid distribution and contours of ratio of grid-scale D and estimated Taylor's micro-scale (λ), along with $Q = 100$ contour line. Grid distribution and contours of ratio of grid-scale D and dissipation length scale (η), along with $Q = 100$ contour line.

(c) For section S2, an additional zoom in view of the grid distribution w/ flooded contour of the ratio of turbulence macro-scale (L) and grid-scale D , and contour line of $y^+=30, 100, 300$ and 1000 , should be provided. Sample figure shown in Figure A.4. y^+ can be estimated using the averaged wall shear stress at section S2 if the solver does not provide y^+ calculation using local wall shear stress and wall normal distance. The domain extent of the three zoomed in views area:

- (i) $y/L = [0, 0.011], z/L = [-0.06, -0.05]$
- (ii) $y/L = [0.005, 0.016], z/L = [-0.045, -0.035]$
- (iii) $y/L = [0.015, 0.023], z/L = [-0.02, -0.0125]$

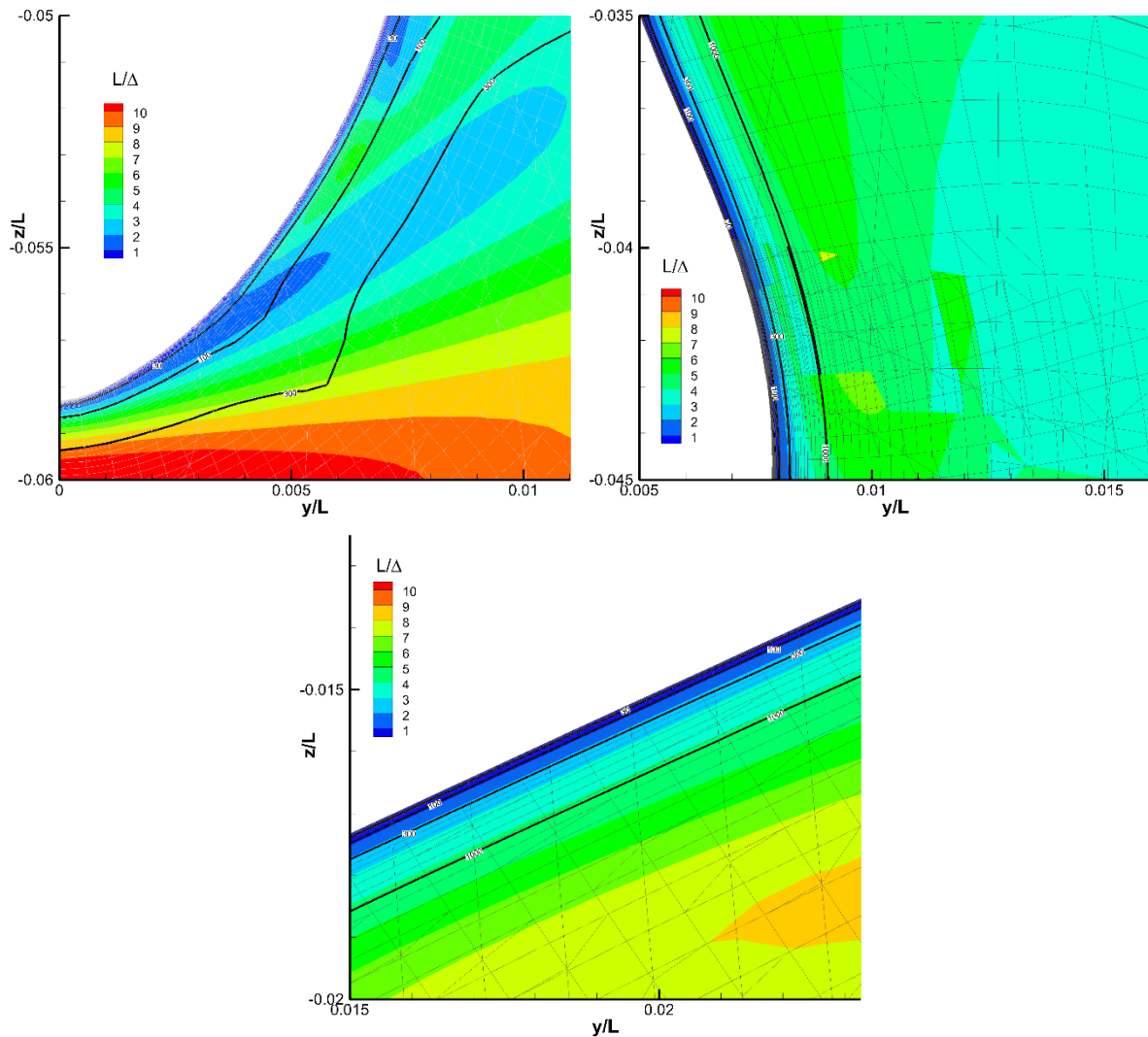


Figure A.4: Zoomed in view of the grid distribution colored using contours of ratio of turbulence macro-scale (L) and grid-scale D , and contour line of $y^+ = 30, 100, 300$ and 1000 . Plot shown at $y/L_{pp} = 0.9825$ plane. Zoomed in location shown in Figure A.3(a).

0.2 Iterative convergence of the solution¹¹

Iterative convergence, i.e., variation of the residual with respect to inner iteration within each time step, help evaluate the effect of iterative errors on predictions. For RANS simulations these will provide the iterative uncertainty, whereas for SRS it will help evaluate if the solution converges sufficiently within each time step to ensure that the solution is not affected by iterative errors. Ideally, residuals for each primary variable should decay to 10^{-5} or 10^{-6} within each time step, before the solution is marched to the next time step. In addition, it should be confirmed that $CFL < 0.5$.

Iterative converge of the CFD simulation within each time step should be shown using the variation of the residual with respect to inner iterations for the primary variables as shown in Figure A.5.

¹¹ Example provided is for implicit solver CFDSHIP-IOWA. If other implicit solvers cannot follow this example similar evidence should be provided using alternative approach. For explicit solvers in addition $CFL < 0.5$, a time step sensitivity should be provided which demonstrates the independence of the time step subject a reasonable tolerance.

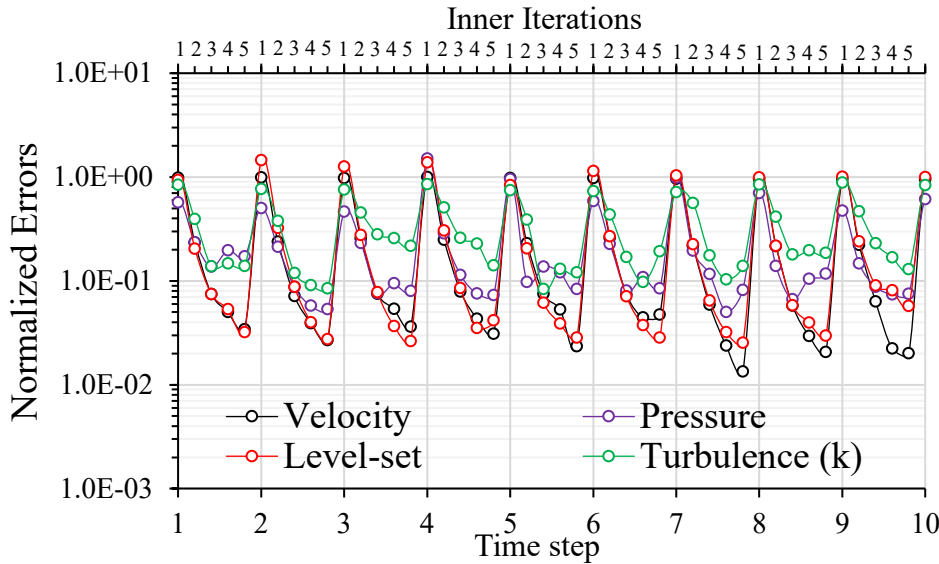


Figure A.5: Normalized residual errors within each time step and inner iteration for primary variables, velocity, pressure, free-surface and turbulence. The errors are normalized by errors of first inner iteration of 1st time step. Residual errors should be preferable computed using L2 norm.

0.3 Integral Variable Solution convergence

Integral variable solution convergence should be shown for forces, moment, and motions, demonstrating that solution either reached quasi-steady state for unsteady prediction or variations decayed sufficiently for steady state predictions. Time running mean should also be performed to demonstrate that mean integral quantities were obtained by averaging over a sufficiently large averaging period.

For this, plots showing entire time history and fully developed region along with running mean should be plotted with respect to solution time (sample plot shown in Figure A.6).

The solution variation in the fully developed region for steady RANS predictions will provide the iterative error in the solution.

The solution variation in the fully developed region for SRS predictions will help evaluate the frequency and amplitude of the large-scale oscillations.

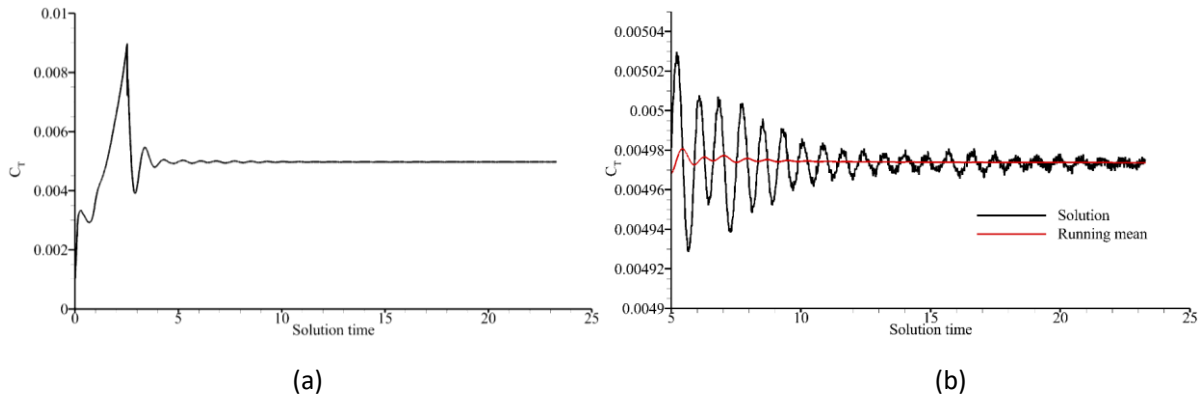


Figure A.6: (a) Time history of the total resistance coefficient predictions over the entire simulation. (b) Total resistance coefficient predictions in converged solution along with running mean.

0.4 Statistical convergence of SRS results

Mean and turbulent flow statistical convergence will help evaluate if averaging is adequate in SRS. The proof of statistical convergence must be presented following the procedures outlined in Yoon et al. (2015) using the time signal of desired quantities.

For a stationary random variable x , the confidence interval that the sample mean (\bar{x}) is within the true mean (μ_x) can be estimated from statistical probability:

$$P(|\bar{x} - \mu_x|) \leq cs_x/\sqrt{n}$$

where, s_x is the standard deviation of the sample, n is the sample size and c is the student's t-statistics corresponding to desired confidence interval. c also depends on data distribution. For example, for desired probability $P = 95\%$, a data set that follows normal distribution results in $c = 2$, whereas for datasets for which distribution is unknown $c = 4.5$. In a previous study, Yoon et al. (2015) reported that force predictions follow normal distribution, whereas velocity, moment, draft and pitch failed the normality test. Thus, $c = 4.5$ is used herein.

The statistical convergence analysis should be performed only after the flow has fully developed and reached a quasi-steady state (when forces, moment and motions show unsteadiness over a mean value) and carried out over a time interval of at least $2L_{pp}/U_\infty$. To evaluate the convergence, the mean values (\bar{x}) and their standard deviation (s_x) of desired quantities should be computed, which are defined as:

$$\bar{x} = \frac{1}{n} \sum_{i=1}^n x_i$$

$$s_x = \sqrt{\frac{1}{n} \sum_{i=1}^n (x_i - \bar{x})^2}$$

where $n = 1, \dots, N$, with N equal to the total number of the simulation time steps and x_i is the quantity at the i -th time step. The statistical convergence error is computed as:

$$E_{sc} \% = \frac{4.5s_x}{\sqrt{n}} / \bar{x} \times 100$$

The statistical convergence error % is then plotted against the increasing number of time steps, as in Figure A.7.

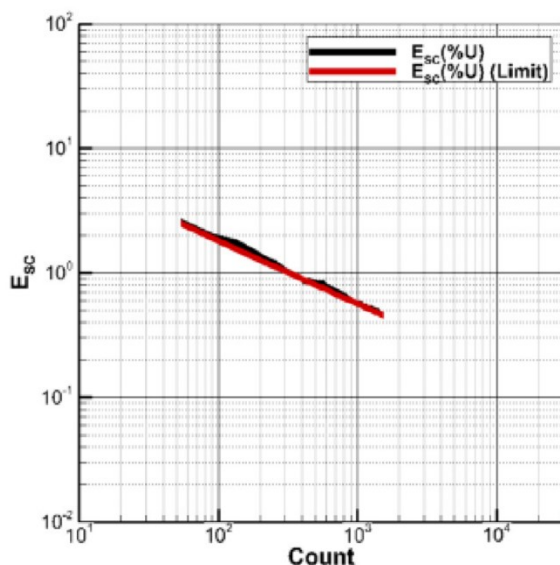


Figure A.7: Proof of statistical convergence of the experimental results for velocity at the core for $N=1500$ samples (Figure taken from Sanada et al., 2023).

Plots should be provided for:

- (a) Time history plot of the axial velocity and resolved TKE along with the running mean in ABVI and ABV2 cores at S4, demonstrating achievement of quasi-steady flow behavior, and the averaging period should be identified in the plot.
- (b) Statistical convergence of mean velocity resolved TKE in ABVI and ABV2 core at S4.

0.5 The SRS deficiency/error analysis

The grid induced separation, and improper shielding can be evaluated by comparing RANS and SRS results, wherein the RANS grid should be the same as that used for the SRS. Grid induced separation occurs when the mean flow shows separation in SRS, even though the RANS results does not. Comparing the mean velocity profile in RANS and SRS will show how well the boundary layer is retained in SRS. The comparison of TKE profiles predicted by RANS with SRS modeled and resolved TKE profiles will provide a measure of the accuracy of the shielding. The SRS modeled TKE should compare well with RANS TKE in the boundary layer, and then slowly decrease while the resolved TKE should increase. The y^+ location where SRS modeled TKE starts to deviate from RANS TKE gives the location of shielding. If the modeled TKE in SRS is larger than those in the RANS, it is a sign of grid induced separation, i.e., excessive energy is being transferred from mean momentum to turbulence.

This analysis needs to be done in the region of interest, i.e., $x/L = 0.5, S1, S2, S3,$ and $S4$. The required analysis is as follows.

- (a) Longitudinal distribution of viscous and pressure girthwise integrated resistance.
- (b) Iso-surfaces of the RANS and grid-scale ratio or DES shielding function focusing on wake region aft of S1, that demarcates the RANS and LES regions, providing a global view of the LES active region. PANS does not have a specific shielding function, so the ratio of modeled to RANS TKE can be used as a surrogate for the shielding function. (Sample Figure A.8).

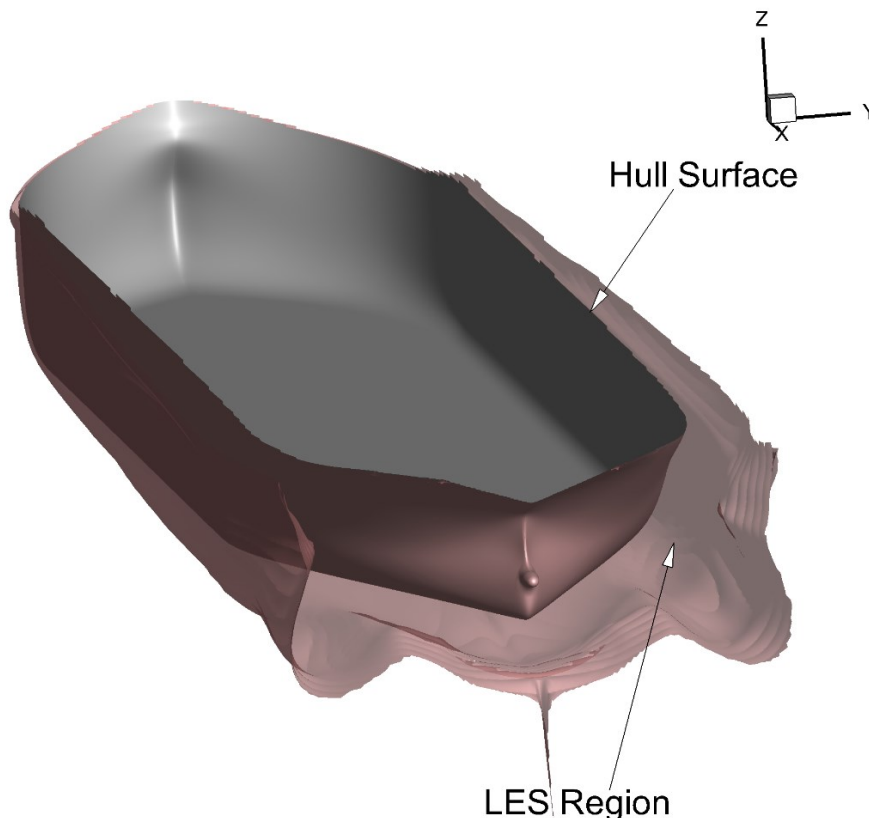


Figure A.8: Iso-surface of DES length-scale ratio $f_d=1$ showing the region where LES is active.

(c) 2D slices at section $x/L = 0.5$, S2, S4 and S7 showing contour of scale ratio and shielding function, showing the transition of RANS to LES in the boundary layer region.

- (i) Plot should show the entire domain of interest (Figure A.9(a)).
- (ii) Zoomed in view at section S2 along with contour lines of $y^+ = 30, 100, 300$ and 1000 to show when the RANS-to-LES switch happens in the boundary layer (Figure A.9(b-d)).

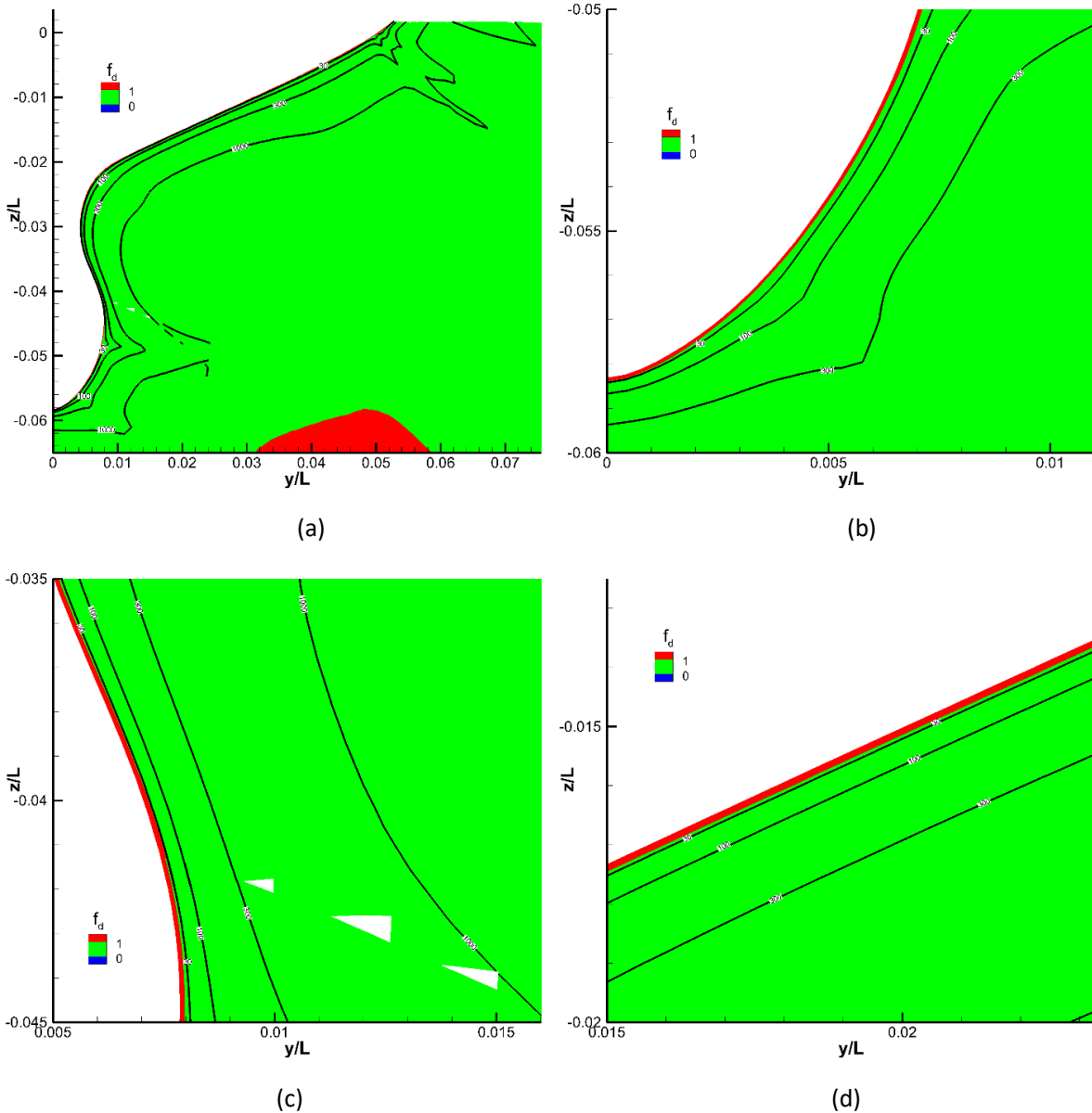


Figure A.9: (a) DES length-scale ratio $f_d = 1$ showing the region where LES is active. Region $f_d \geq 1$ is RANS region, and $f_d \leq 1$ is LES region. Contour lines of $y^+ = 30, 100, 300$ and 1000 . (b-d) Figure 0.1.3. Plot shown for the zoomed in view in Figure A.3(a).

- (iii) 2D slices at above sections showing resolved and modeled TKE levels.
- (iv) Line cuts at one location at S1 ($x/L = 0.95$) (Figure A.10) and three locations at S2 ($x/L = 0.9625$) (as shown in Figure A.11, Figure A.12 and Figure A.13) comparing HRLES and RANS mean velocity and TKE in the boundary layer, and ratio of RANS TKE and HRLES modeled

TKE. Line cut locations are included in the Excel file 0.5.c.iv.Line-Cuts.xlsx which can be downloaded from the website

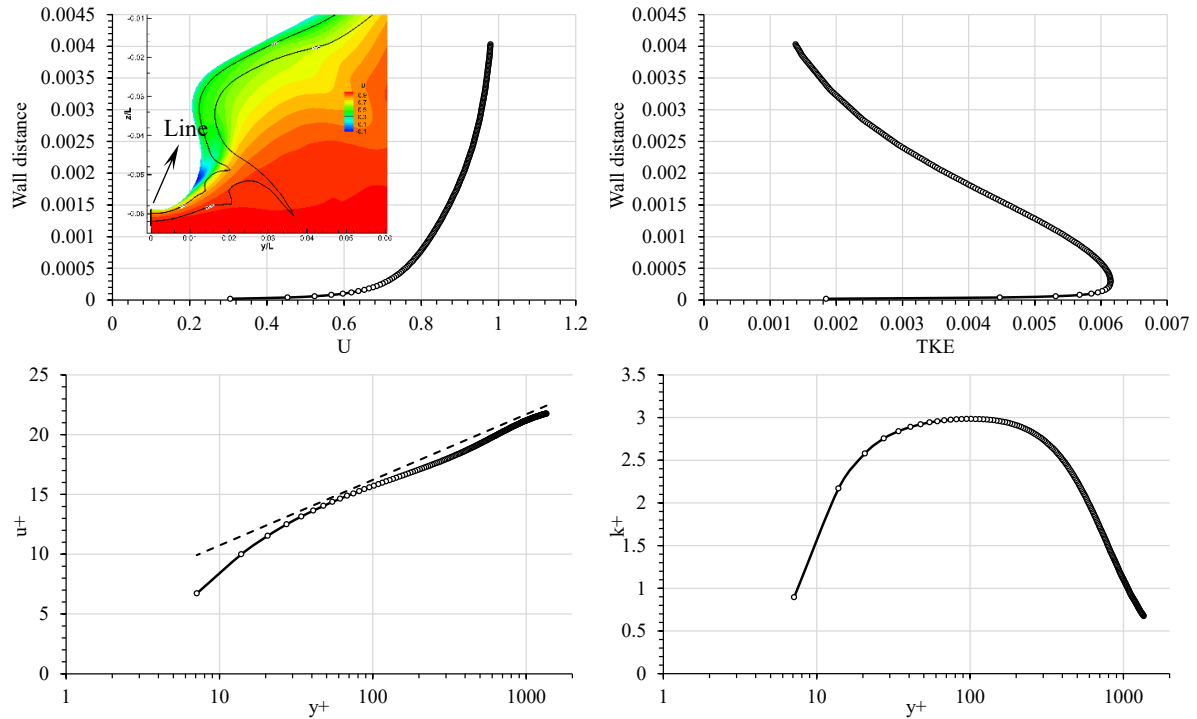


Figure A.10: Axial velocity and TKE are plotted with respect to wall distance (top panel), velocity magnitude and TKE are normalized using friction velocity and plotted in wall units (bottom panel). Normalized velocity profile is compared with log-law (broken line). The coordinates for the line-cut are specified in the Excel file on the website.

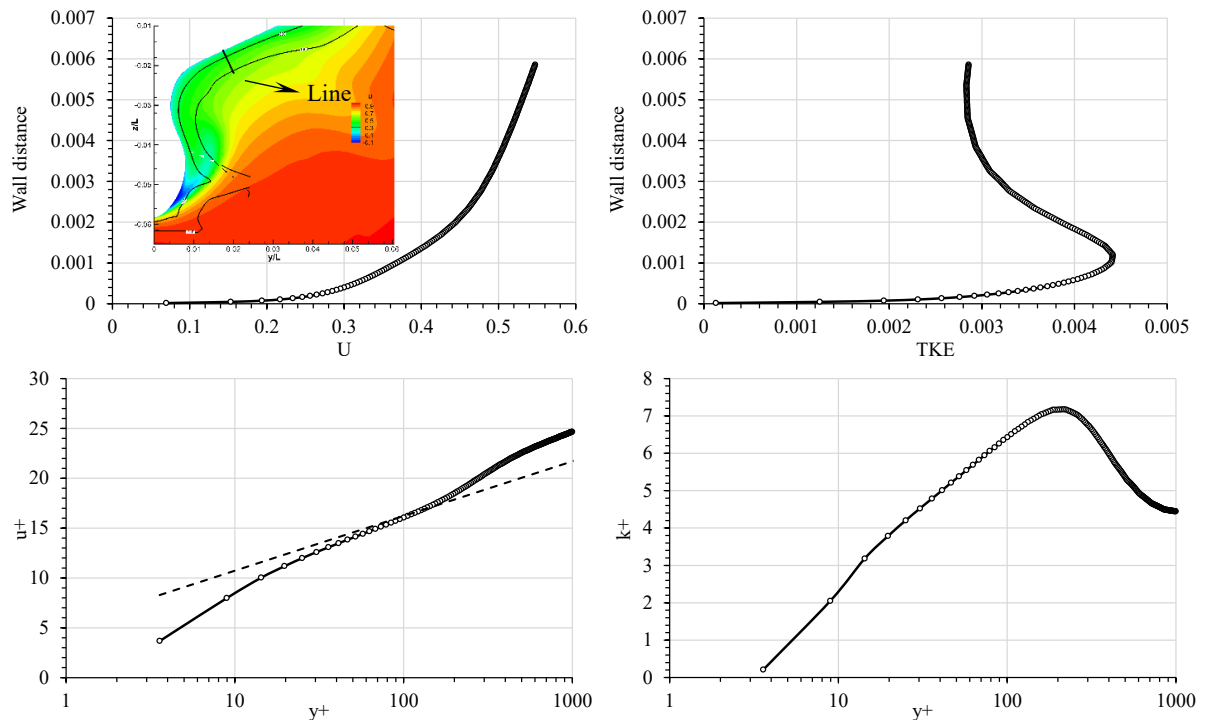


Figure A.11: Axial velocity and TKE are plotted with respect to wall distance (top panel), velocity magnitude and TKE are normalized using friction velocity and plotted in wall units (bottom panel). Normalized velocity profile is compared with log-law (broken line). The coordinates for the line-cut are specified in the Excel file on the website.

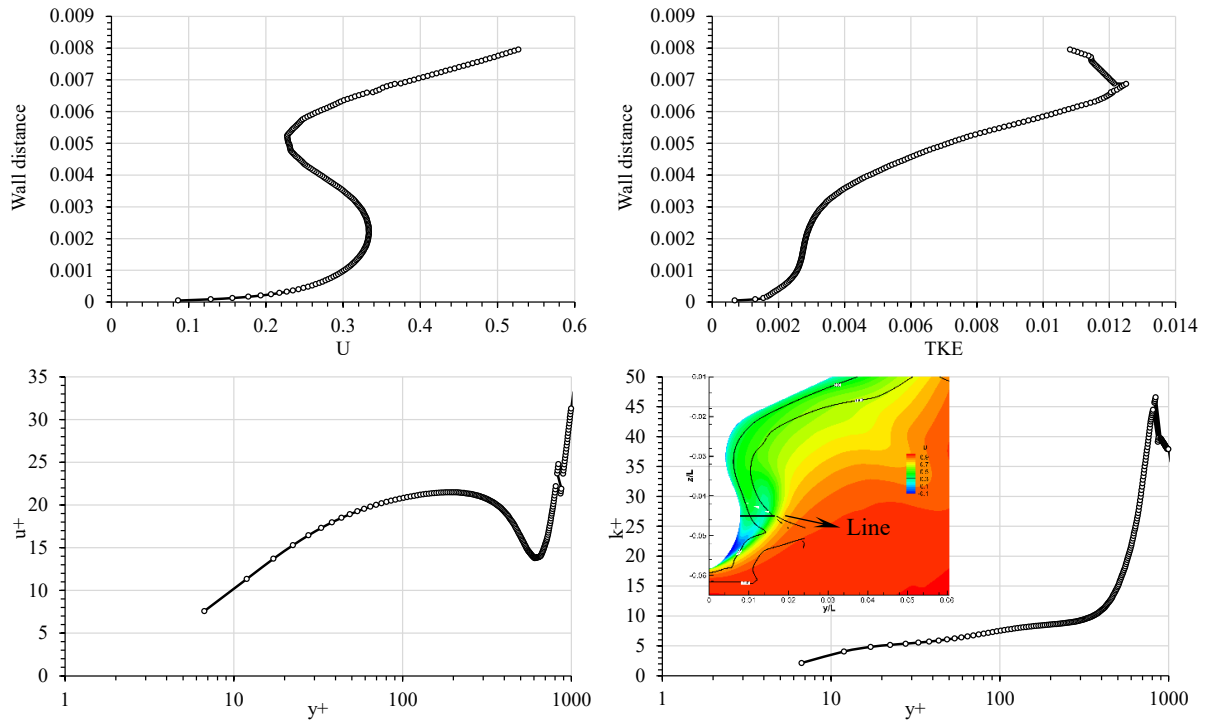


Figure A.12: Axial velocity and TKE are plotted with respect to wall distance (top panel), velocity magnitude and TKE are normalized using friction velocity and plotted in wall units (bottom panel). Normalized velocity profile is compared with log-law (broken line). The coordinates for the line-cut are specified in the Excel file on the website.

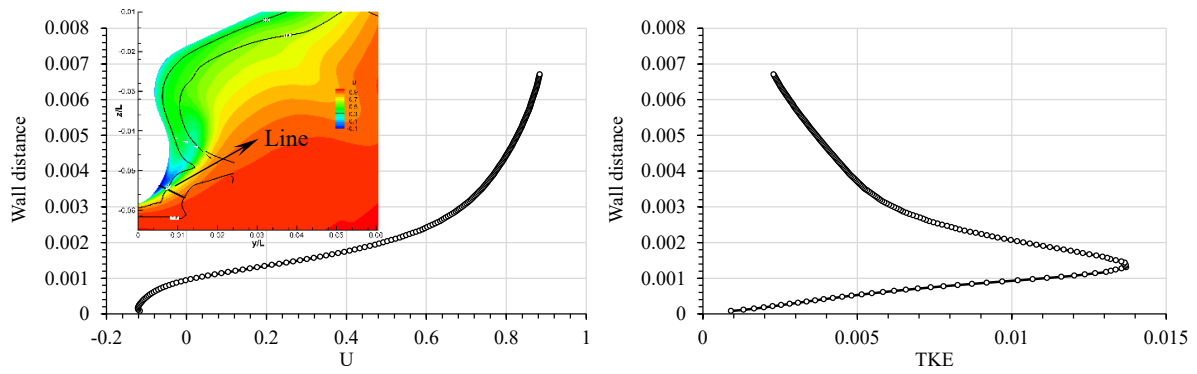


Figure A.13: Axial velocity and TKE are plotted with respect to wall distance.

Nomenclature

Hull Parameters

X, Y, Z	Coordinate direction along axial, spanwise and normal direction, respectively
$L_{pp}(m)$	Length between perpendiculars
$L_{WL}(m)$	Length of waterline
$B_{WL}(m)$	Maximum beam of waterline
$\nabla(m^3)$	Displacement volume
$D(m)$	Depth
$T(m)$	Draft
$S(m^2)$	Wetted surface area
C_B	Block coefficient
C_M	Midship section coefficient
LCB ($\%L_{pp}$)	Forward of midship
KB (m)	Vertical center of gravity (from keel)
S	Hull wetted area
z	Sinkage (+ upward)
θ	Trim (+ bow-up)

Flow Parameters

$V_m(m/s)$	Model speed
$(U, V, W)/V_m$	Flow velocity along axial, spanwise and normal direction, respectively
$c_p = \frac{p - p_0}{0.5\rho V_m^2}$	Dynamic pressure coefficient
$F_n = \sqrt{V_m/gL_{PP}}$	Froude number
$R_n = V_m L_{PP}/\nu$	Reynolds number
R_T, R_P, R_F	Total resistance, pressure resistance and frictional resistance, respectively.
F_Z	Vertical hydro force
M_y	Pitching moment
$C_T = R_T/1/2\rho V_m^2 S$	Total resistance coefficient
C_w	Wave making resistance coefficient
$C_P = R_P/1/2\rho V_m^2 S$	Pressure resistance
$C_F = R_F/1/2\rho V_m^2 S$	Frictional resistance
C_{F0}	ITTC 1957 correlation line for frictional resistance
$\tau_w = \mu \frac{\partial u_t}{\partial n}$	Wall shear stress based on wall normal derivative of hull tangential velocity $(\frac{\partial u_t}{\partial n})$
Ψ_0	Surface streamlines
$g = 9.80 m/s^2$	Acceleration due to gravity
$r (kg/m^3)$	Water density
$\nu \left(\frac{m^2}{s}\right)$	Kinematic viscosity
QL^2/V_m^2	Second-invariant of rate-of-strain tensor
Q_{peak}	Maximum value of Q at vortex core

Turbulence Parameters

$\langle U \rangle, \langle V \rangle, \langle W \rangle$ [m/s]	Time averaged axial, spanwise and normal velocities, respectively
$u' = U - \langle U \rangle, v' = V - \langle V \rangle, w' = W - \langle W \rangle$	Turbulent velocity fluctuations
$\frac{\langle u'u' \rangle}{v_m^2}, \frac{\langle v'v' \rangle}{v_m^2}, \frac{\langle w'w' \rangle}{v_m^2}, \frac{\langle u'v' \rangle}{v_m^2}, \frac{\langle u'w' \rangle}{v_m^2}, \frac{\langle v'w' \rangle}{v_m^2}$	Reynolds stress components
$\langle u^2 \rangle = \langle u'u' \rangle$ [m ² /s ²]	Root-mean-square axial velocity fluctuation
k [m ² /s ²]	Turbulent kinetic energy
k_{mod}	Modeled TKE
$k_{res} = \frac{1}{2} (\langle u'^2 \rangle + \langle v'^2 \rangle + \langle w'^2 \rangle)$	Resolved TKE
$u'_{TI} = \sqrt{\frac{2}{3}} k \left(\frac{m}{s} \right)$	Turbulence intensity
L [m]	Largest energy containing length scale Estimated based on diameter of vortices, ABV1 and ABV2, based on $\frac{1}{2} Q_{peak}$ Estimated based on (URANS), $\approx \frac{k^{3/2}}{\varepsilon}$
$\varepsilon = k^3/L$ [m ² /s ³]	Molecular dissipation
$Re_L = \frac{\sqrt{k}L}{\nu}$	Turbulent Reynolds number
λ_f [m] = $L\sqrt{20/Re_L}$	Taylor's micro-scale
Λ_f [mm] = $\frac{3\pi}{4k} \int_0^\infty \frac{E(k)}{k} dk$	Taylor's macro-scale based on energy spectrum
$R_\lambda = \frac{\sqrt{k}\lambda_f}{\sqrt{2}\nu}$	Taylor's micro-scale based on Reynolds number
η [m] = $\left(\frac{\nu^3}{\varepsilon} \right)^{\frac{1}{4}}$	Kolmogorov's dissipation length-scale
$h = LRe_L^{-3/4}$	Estimated Kolmogorov's dissipation length-scale for grid-scale analysis
$D = \sqrt[3]{V}$	Grid scale, where V is grid volume.
$L_{EI} = \frac{1}{6} \frac{k^{3/2}}{\varepsilon}$	Length-scale marking the lower end of the energy-containing range and start of the inertial subrange

Non-dimensional Quantities

$u_\tau = \sqrt{\tau_w/\rho}$	Friction velocity
$u^+ = U /u_\tau$	Velocity magnitude normalized in wall units, where $ U = \sqrt{\langle U \rangle^2 + \langle V \rangle^2 + \langle W \rangle^2}$
$y^+ = y_w u_\tau/\nu$	Normalized wall distance (y_w)
$k^+ = k/u_\tau^2$	Normalized TKE

Document Revisions

- 2025-01-28: Initial version for the website.
- 2025-01-30: Corrections of typos, and specification of line cut locations as asked in 0.5(c) iv.